Transverse periodic $\mathcal{PT}$ symmetry for modal demultiplexing in optical waveguides

Henri Benisty,[1,*] Anatole Lupu,[2,3] and Aloyse Degiron[2,3]

[1]*Laboratoire Charles Fabry, Institut d'Optique, CNRS, Université Paris-Sud, 2 Avenue Augustin Fresnel, 91127 Palaiseau, France*
[2]*Université Paris-Sud, Institut d'Electronique Fondamentale, UMR 8622, 91405 Orsay Cedex, France*
[3]*CNRS, Orsay F-91405, France*

Multimode waveguides can be used as multichannel devices to push the transmission bandwidth of optical signals to its limits, provided demultiplexing can be correctly performed, e.g., by selecting a given mode from the rest of the modes. This simple task is usually accomplished by Fourier filtering and requires long interaction distances; here we propose a possibly more compact alternative by using parity-time ($\mathcal{PT}$) symmetry in a periodic fashion in the transverse direction, laying out stripes with gain and losses across the guide width. We first describe the evolution of the system as the level of gain and losses varies and then provide a perturbation analysis of the waveguide mode eigenvalues that clarifies this behavior. We next show that this stripe pattern results in a configuration of eigenvalues that can select a narrow subset of modes. We outline the close relationship between a simplified tight-binding model for an array of coupled single-mode waveguides and a genuine broad multimode dielectric waveguide, showing the advantage of the simplified model for quick studies exploring the complex landscape of $\mathcal{PT}$ symmetry in multimode waveguides.

I. INTRODUCTION

Parity-time ($\mathcal{PT}$) symmetry was introduced in the usual Hermitical Hamiltonians by adding balanced imaginary contributions to their diagonal elements and remarking that within a given range of this contribution, the operators retained real eigenvalues [1,2]. The evolution to complex eigenvalues further leads to symmetry breaking of the two eigenmodes, occurring at an exceptional point. In optics, applications of $\mathcal{PT}$ symmetry can be naturally targeted as the imaginary contributions are gain and loss, that have to appear in a parity-symmetric fashion, such as $\varepsilon(x,y,z) = \varepsilon^*(-x,y,z)$: This condition on a dielectric map $\varepsilon(x,y,z)$ corresponds to a symmetric real dielectric constant and an antisymmetric imaginary dielectric constant, transforming gain into loss upon symmetry, e.g., $\mathrm{Im}[\varepsilon(x,y,z)] = -\mathrm{Im}[\varepsilon(-x,y,z)]$, such examples having a symmetry plane at $x = 0$.

Numerous developments of multiple-element $\mathcal{PT}$-symmetry systems (PTSSs) have appeared in the past few years, especially in relation with optics [3–30]. Practical implementations can relax the requirement of exact gain-loss antisymmetry, for instance in so-called passive $\mathcal{PT}$-symmetric systems with variable losses but no gain [5–7] or in plasmonics where considering fixed losses is a reasonable starting point [8–10]. Most optics-related studies have favored, as the linear-physics basis of their work, the two flavors of $\mathcal{PT}$ symmetry that we itemize and illustrate in Figs. 1(a) and 1(b).

The first of these configurations, represented in Fig. 1(a), has been introduced in 2005, by Kulishov *et al.* It consists of a periodic $\mathcal{PT}$-symmetric potential along the propagation direction of a waveguide with implications, such as "spatial nonreciprocity," in the form of a complete difference in reflection from the two sides of the device [11]. This flavor of $\mathcal{PT}$ symmetry [11–14] has recently been experimentally implemented in its passive form (i.e., without gain) in multi-layer systems based on silicon [28] or organics [7], whereas a waveguide implementation using two different modes has also been a milestone of $\mathcal{PT}$-symmetry applications in optics [15].

At variance with this "longitudinal" $\mathcal{PT}$ symmetry, a simple "transverse $\mathcal{PT}$" studied system consists of two waveguides carrying gain and loss, respectively, and coupled together by simple proximity as schematically shown in Fig. 1(b) [16,17]. The physics is simpler since only co-directional coupling is involved. An experimental demonstration reported by Rüter *et al.* in 2010 [16] provided a striking milestone of $\mathcal{PT}$ symmetry in optics, going beyond the "passive-$\mathcal{PT}$-symmetric systems" of earlier examples. In parallel, the related case of lattices of waveguides has also been vigorously investigated by several authors [17–22,26,27,29–34]. We will indeed use such a lattice as discussed later, noticing that in some cases in Refs. [30–34], there are analytical results for the exceptional points that could serve in further studies.

Still, it is a distinct flavor of $\mathcal{PT}$ symmetry that we wish to introduce in this paper—a periodic variation in gain and loss applied to the transverse direction of a multimode waveguide as seen in Fig. 1(c). Besides an academic interest, the study is motivated by the capability of such multimode broad waveguides to serve as multichannel high-rate links for datacom notably. A guide of the width of a couple of microns may easily carry ten channels in a high-index core to give an idea of the potential of this approach. To extract a stream of data of a given channel from such systems, there are several possibilities. What is generically needed is some kind of spectrometer that takes into account the dispersion of the transverse wave vector inside the waveguide to select a channel. One can distinguish conservative and nonconservative approaches.

The conservative framework is well exemplified by the multimode interferometer (MMI) approach, a workhorse of integrated optics [35,36]. Still, in such a case, there is a need to physically modify the boundaries of the waveguide at the
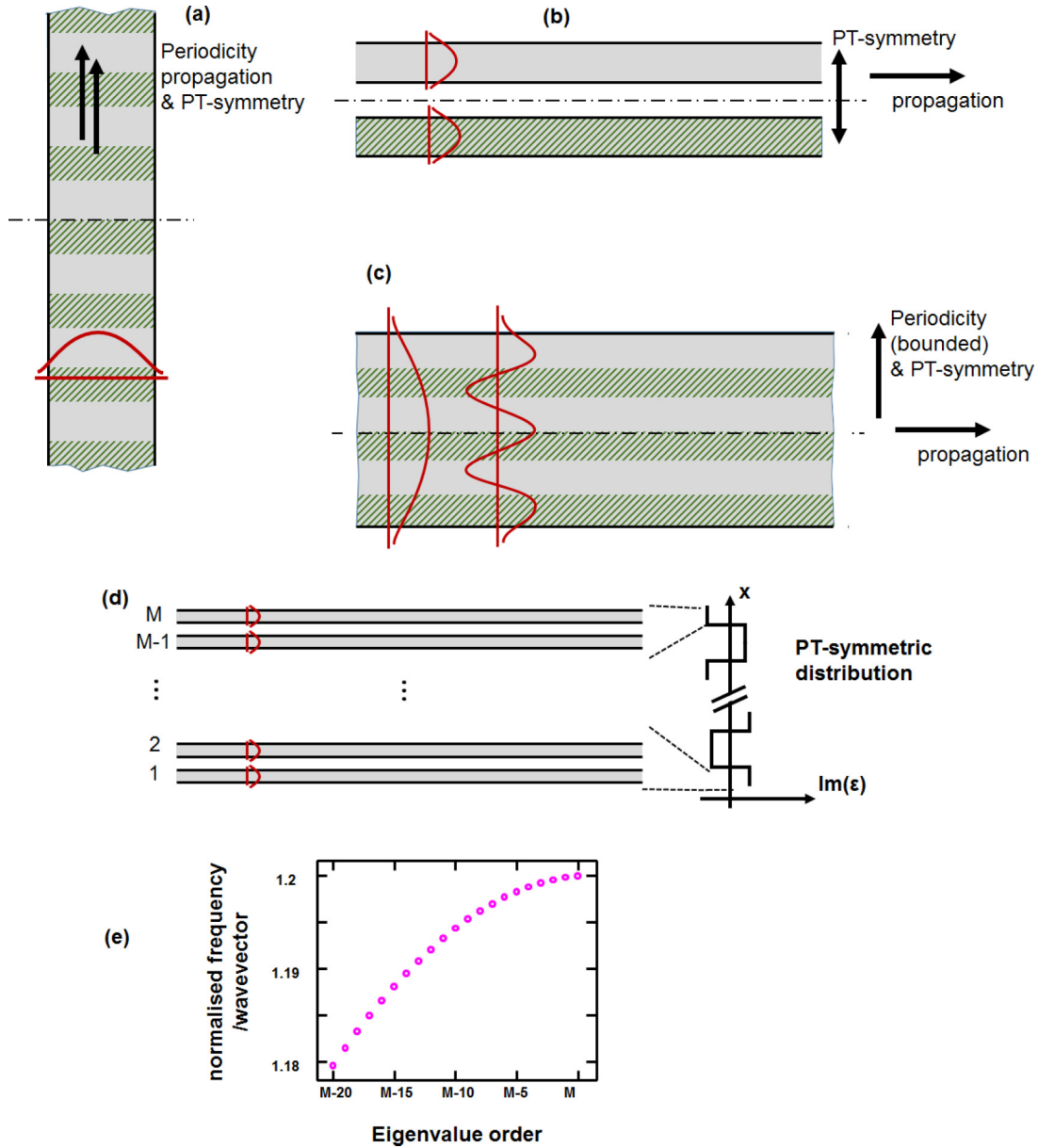
---

*henri.benisty@institutoptique.fr

FIG. 1. (Color online) $\mathcal{PT}$SSs: (a) longitudinal $\mathcal{PT}$SS, (b) transverse $\mathcal{PT}$SS made of two distinct guides, (c) multimode transverse guided $\mathcal{PT}$SS, (d) multiple coupled waveguide model as an approximation of the broad waveguide, and (e) the eigenvalue distribution close to the band edge has a quadratic evolution, just as successive guided modes of a broad waveguide.

analyzer side such that the data stream is disrupted: It cannot constitute a tunable device, choosing which channel to analyze or offering, e.g., to switch between an analysis mode and a blank "through" mode for all channels. Other methods for modal demultiplexing (without MMI) have considered that a generic solution could be obtained by defining a scatterer from simple basic units, such as round "atoms" [37] or other emerging schemes [38,39]. Even though they are not commonly discussed, it is clear that conservative approaches that fully disperse the transverse momentum spectrum and reconstitute new channels, akin to add-drop filters in the frequency domain, tend to be bulky: a lot of free space or, equivalently, an arrayed-waveguide-grating-type (phasar) device is required to perform the Fourier analysis of the combined mode wave fronts inside the guide.

Nonconservative approaches work by imposing tunable loss or gain patterns to select targeted modes. They may have the advantage of tunability, especially when guidance is supported by a high-index-contrast system or by a plasmonic system, whose index tuning to implement the Fourier or conservative strategies is difficult if not impossible to achieve.

The simplest nonconservative approach is relatively obvious: It consists of forming a transverse gain profile $g(x)$ that matches the targeted mode intensity profile $g(x)$: Ideally $[g(x) - g_o] \propto |E(x)|^2$ with a given bias gain g_o [g_o may be negative: It then represents a given bias loss, allowing, for instance, a zero mean for $g(x)$]. Because such approaches have the same even P symmetry as $|E(x)|^2$, they cannot be $\mathcal{PT}$ symmetric. Their specific exploration for datacom has yet to be performed, and there is a limited amount of

mystery in this approach because it corresponds to the issue of parasitic (generally higher-order) mode amplification in any active multimode device, laser, or amplifier. Filamentations in highly pumped media and modulation instabilities are typical nonlinear phenomena related to the amplification and saturation among higher-order transverse modes of slab or fiber waveguides.

In this paper, we adopt a nonconservative strategy based on $\mathcal{PT}$ symmetry to select one or very few modes from a multimode waveguide with, ideally, maximum selectivity. Although $\mathcal{PT}$-symmetry effects on two separate waveguides is well documented, studies of multimode systems with some implementation of $\mathcal{PT}$ symmetry have focused so far on separate coupled elements [17–22,26,27,29–34] rather than modes of a single multimode waveguide. And they have not considered the capability to specifically amplify a subset of modes. Furthermore, our previous work on plasmonic systems with $\mathcal{PT}$ symmetry [8–10,14] has suggested that $\mathcal{PT}$ symmetry may offer a unique situation of "large differential gain" in the vicinity of exceptional points, whereby the imaginary part of the eigenvalues evolves faster than elsewhere in dispersion diagrams. This may provide opportunities to amplify a subset of modes having an exceptional point (EP) in that parametric region comparatively to all other modes, typically a pair of modes.

However, before getting the specific modal amplification trends suggested above, it is useful to find tools that result in a quick treatment of the main effects of $\mathcal{PT}$ symmetry in broad waveguides. This will be a central point of our study, and we will consider to this aim an array of individual oscillators (that can be seen as single-mode waveguides) coupled only via a first-neighbor (FN) interaction. Although such a tight-binding system has been popular as a model for transport studies [26], for instance in light localization studies among other things, it has not been much used as a tool for multimode physics in a given broad waveguide. We propose here a use of this system to easily get the response of the broad waveguides submitted to a $\mathcal{PT}$-symmetric distribution of gain and loss. We check which of the features obtained in this simple system correspond to an actual slab waveguide having a gain or loss distribution with odd parity. We propose ways to bridge both systems and use the simplified generic system to carry out a first modal discrimination study.

The paper is organized as follows. In Sec. II, we present the general properties of $\mathcal{PT}$-symmetric multimode waveguides, typically with index contrast 2.8/1 to mimic silicon-on-insulator (SOI) generic structures. In Sec. III, we justify these results with the simplified FN coupled array mentioned above. We subject this simpler model to $\mathcal{PT}$ symmetry and examine the resulting shift of its eigenvalues by means of a second-order perturbative analysis, revealing the underlying physics through basic matrix elements and associated selection rules. In Sec. IV, we discuss the exact diagonalization and the exceptional points of the FN coupled array, and we show, in the same section, how to modify the $\mathcal{PT}$-symmetric perturbation profile with some physical insight to fit the behavior of an actual system. In Sec. V, we use the simplest form of transverse $\mathcal{PT}$ symmetry to show an example of modal discrimination in a true multimode waveguide before concluding in Sec. VI.

II. BROAD DIELECTRIC WAVEGUIDE WITH TRANSVERSE $\mathcal{PT}$ SYMMETRY

We consider here a broad waveguide operated at a wavelength λ, of core index having a real part of $n = 2.8$, and whose thickness is $W = 6\lambda$, surrounded by index $n = 1.0$. In practice, it could be a channel waveguide in the SOI technology, the cladding index being not crucial to the study. For $\lambda = 1.55\,\mu$m, it would have a width of 9.3 μm and would support some 30 guided modes in the TE polarization, the sole polarization studied here (electric field parallel to boundaries). A typical application would envision using the 15 lowest order modes that lie within an effective index range [2.4–2.8] that is high enough, hence with limited and well-known dispersion effects (the group index remains rather low) compared to the next higher-order modes.

The $\mathcal{PT}$-symmetric modulation consists of applying on the slab a gain or loss modulation having antisymmetry with respect to the guide symmetry plane. The total number of periods is N, where $2N$ is the number of slab gain regions and loss regions across the transverse width W of the waveguide, Fig. 1(c). From here on we freeze the vertical dimension of the waveguide and consider only a two-dimensional geometry with an Oz waveguide direction as the symmetry line and a transverse axis Ox. In other words, we are essentially interested in dielectric maps $\varepsilon(x)$ whose real part is x symmetric and whose imaginary part is antisymmetric.

It is classical in such an integrated optics configuration to first think in terms of a perturbation approach whereby the modal gain of the mth mode is the weighted product of its unperturbed profile by the gain profile: $g_m \equiv \int |E_m(x)|^2 g(x)dx$. This is a useful guide but will not be valid when we approach the exceptional point and the symmetry-breaking points. Still, it can help forecasting the fact that the compound gain + mode profiles are determining the phenomenology. In the zero-average gain situation [$\int |E_m(x)|^2 g(x)dx = 0$], it thus tells us that a zero modal gain does not only stem from the interaction of an even mode with an odd gain profile, but also the other way round, which opens up the possibility of exceptional points in a non-$\mathcal{PT}$-symmetric dielectric map $\varepsilon(x)$. The full perturbative approach made in Sec. III on the simplified FN model will go more in depth.

Our study of the dielectric waveguide in this section goes as follows.

Let us denote $\varepsilon_R(x)$ as the slab index profile of value $n^2 = 7.84$ in the x interval [$-W/2\ W/2$] and 1.00 outside this interval. We look for the poles of the transmission matrix U along x of such a system by calculating such matrices on the complex k_z plane when varying the gain or loss parameter $\Delta\varepsilon_I$ that defines the dielectric map according to the following form:

$$\varepsilon(x) = \varepsilon_R(x) + i\,\Delta\varepsilon_I f(x). \tag{1}$$

Here, $f(x) \equiv \text{sgn}[\sin(6\pi x/W)]$ is our simple choice, with sgn as the sign function: a square modulation exactly as that of Fig. 1(c), odd vs x. We use either clever pole hunting or mere scanning as exceptional points are tricky. We represent the pole or generally the k_z values by their effective index, i.e., their normalized value $n_{\text{eff}} = k_z/k_o$, where $k_o = \omega/c$ is the vacuum wave vector of light at frequency $\omega/2\pi$.
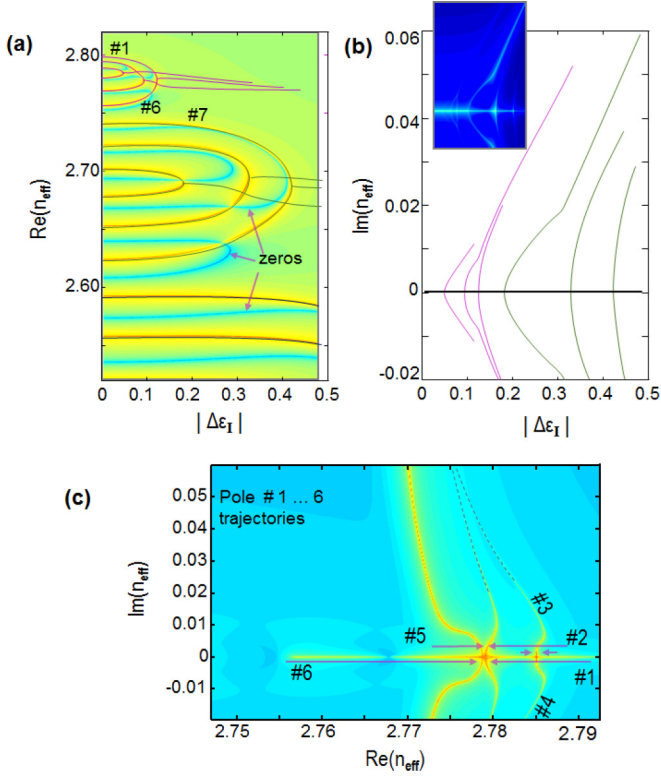
FIG. 2. (Color online) (a) Branches of $Re(n_{eff})$ vs gain or loss denoted $\Delta\varepsilon_I$. The background shows a color image of $\log_{10}[|U_{11}|]$ where bluish lines are the zeros, (b) branches of $Im(n_{eff})$ vs gain or loss; the inset shows a color image of $\log_{10}[|U_{11}|]$, (c) complex plane trajectory of n_{eff} for varying gain or loss in the range $0 \rightarrow 0.2$. The six first mode trajectories are labeled. They are shown by a magenta line color in (a).

The results are displayed in Fig. 2. Figure 2(a) shows the evolution of $Re(n_{eff})$ vs $\Delta\varepsilon_I$, Fig. 2(b) shows the evolution of $Re(n_{eff})$, and Fig. 2(c) shows the complex plane trajectory. See for instance Refs. [8,9] for such trajectories in other real systems.

We can see in Fig. 2(a) that the original modes of the ideal guide form clusters grouping six of them. The patterns share a nearly identical topology whereby the first EP (merging of two real indices) is surrounded by two additional merging events occurring at slightly higher $|\Delta\varepsilon_I|$, the real part of the branches thus formed being isolated from the next adjacent cluster. In the imaginary part diagram, we see the successive branching, but the clusters cannot be isolated from this perspective, even though each set of 2×3 branches (complex conjugate branches) corresponds to a cluster. In the complex plane evolution diagram of Fig. 2(c), we grasp more clearly the complexity of the evolutions of the real part, with several "serpentine" branches corresponding to a nonmonotonous evolution of the real part, first downward due to the generic coupling effect by the gain or loss, then upward when real parts are merged together after the third rightmost EP of each cluster. Similarly, the second and third EPs of each cluster in Fig. 2(a) do not coincide with the largest imaginary part of the branches before merging (before symmetry breaking of the eigenmodes).

All these specific patterns are nevertheless illustrative of more universal features. For instance, the six-mode clusters are intimately related to the $2N = 6$ stacked media, and we can conjecture that slicing the guide into N periods of $\mathcal{PT}$-symmetric nature results in clusters of $2N$ modes. Yet, it would be instructive to have a toy model to depict the eigenvalue behavior. Tracking the eigenvalues across EPs or across accidental zeros of the transmission matrix coefficient, such as the one indicated at around $n = 2.635$, is difficult. If a low-order eigenvalue problem can be defined that has similar properties, all the corresponding studies can be accelerated, and the understanding of the use of $\mathcal{PT}$SS to accomplish a number of useful tasks can be more efficiently explained and exploited. This is what we do in the next section.

III. THE FIRST-NEIGHBOR WAVEGUIDE ARRAY PARITY-TIME SYMMETRIC MODEL

The simplified model that we propose consists of an array of M basically identical monomode waveguides ($j = 1\ldots M$, each mode being denoted $|j\rangle$), coupled between nearest neighbors only, Fig. 1(d). Their only difference comes from a $\mathcal{PT}$-symmetric perturbation. The evolution operator (Hamiltonian) depicting such an array is a tridiagonal matrix simply expressed as

$$A_{jk} = [\omega_o + i \ \Delta\omega_I f_j]\delta_{j,k} + \kappa[\delta_{j,k+1} + \delta_{j,k-1}]. \quad (2)$$

In other words, all elements are coupled to two neighbors, but the extreme elements of the array have a single neighbor instead. It is well known that such systems in the non-$\mathcal{PT}$ case $\Delta\omega_I = 0$ present bands and were studied in the context of disorder or ordered systems [26,27,29,30,40–44] due to their good embodiment of basic solid-state physics concepts (bands, band edges, transport, etc.). Let us recall that for a constant diagonal term ($\Delta\omega_I = 0$), the eigenvalues of this matrix are located on a band centered at ω_o of width 2κ. They are naturally labeled by a normalized wave vector $q_k = k/2(M + 1)$ ($k = 1, \ldots, M$) into the dispersion relation $\omega_k = \omega_o + 2\kappa \cos(2\pi q_k)$, having the typical quadratic dependence of confined levels near the band edges (BEs) $\omega_{BE} = \omega_o \pm 2\kappa$. The top band edge is shown in Fig. 1(e). The eigenvalues have a quadratic evolution downwards, just as the effective indices of a broad waveguide do. Thus, the index k is a normalized momentum that labels eigenvalues and eigenvectors. These latter have k antinodes in their sine-type profile, reading

$$|k\rangle = \sum_{j=1,\ldots,M} \{B_M \sin[j\pi k/(M + 1)]|j\rangle\}. \quad (3)$$

We took the signs so that the lower eigenvalues correspond to a downward band curvature (since defining and ordering the q_k is somewhat arbitrary) and use arbitrary values $\omega_o = 1$ and $\kappa = 0.1$ to give the appearance of a band dispersing downward from the positively valued band edge $\omega_{BE} = 1.2$ on. So their ordering follows the eigenvalues n_{eff}^2 of the Helmholtz equations. The eigenvalues at the other band edge ($\omega_{BE} = 0.8$) are just symmetrically situated. We will see that the evolutions caused by the imposition of extra $\mathcal{PT}$-symmetric modulations made below are also symmetric at both band edges.

To implement a gain or loss modulation equivalent to the square one of the broad dielectric waveguide above, we impose the $\mathcal{PT}$ symmetry to the f_j sequence around $j = M/2$. To find properties that are independent of the size M, simple symmetry considerations should be used to avoid artifacts. For instance, since we have six equal regions in the example above, $f(x) \equiv \mathrm{sgn}[\sin(6\pi x/W)]$, we take M to be a multiple of 6 to safely implement a sequence $f_j = \pm 1$ made of six subsections each with exactly the same number of elements $j = M/6$. The same principle can of course apply to a higher transverse index with $2N$ subsections, suggesting $M/2N$ to be an integer to correspond to $f(x) \equiv \mathrm{sgn}[\sin(2N\pi x/W)]$.

Before extracting exact solutions in Sec. IV, we present here a perturbative analysis to second order of the eigenvalues. The matrix elements of $i\,\Delta\omega_I\, f_j$ between two eigenmodes $\langle k|$ and $|l\rangle$ involved in second-order eigenvalue perturbations can be written using a continuous function $f(x)$,

$$D_{kl} = \langle |i\,\Delta\omega_I f(x)|l\rangle . \tag{4}$$

And the second-order perturbative shift of eigenvalue ω_I is $\delta\omega_I^{(2)} = \sum_{k \neq 1} |D_{kl}|^2/(\omega_k - \omega_l)$. There is a vanishing first-order term if f has the odd-P parity through the waveguide central plane. We represent as a color map these matrix elements for the 40 first k,l values of a large guide ($M = 204$) in Fig. 3(a) for a case where $N = 3$. It is clear that the pattern then bears the footprint of a sixfold cycle. We will now elucidate this feature with some more generality and show that it essentially amounts to a transverse momentum conservation rule, somehow similar to that met in describing confined phonons interacting with confined electrons in a square profile quantum box [44].

To see this, we replace the discrete sum on $j's$ by $\int dx$, The essential ingredient of D_{kl} then transforms into an integral of the form

$$D_{kl} \propto \int_{-W/2}^{W/2} \sin[\pi k(x + W/2)/W]$$
$$\times \sin[\pi l(x + W/2)/W]f(x)dx. \tag{5}$$

At this stage, we can further simplify the problem by considering the fundamental harmonic of the square periodic function $f(x)$. We can write it, $2N$ being even and $f(x)$ being odd with respect to $x = 0$, $f_1(x) \equiv \sin(2\pi Nx/W)$. Working out the product of the two first sine in the integrand of Eq. (5), we have to calculate

$$D_{kl} \propto \int_{-W/2}^{W/2} \cos[\pi(k - l)(x + W/2)/W]\sin(2\pi Nx/W)$$
$$- \cos[\pi(k + l)(x + W/2)/W]\sin(2\pi Nx/W)dx. \tag{6}$$

Each of the two terms gives rise in turn to terms in $\sin[\pi(k \pm l)(x + W/2)/W \pm 2\pi Nx/W]$. These are sine waves integrated between two of their zeros: one zero at $x = -W/2$ corresponding to the argument $\mp N\pi$ and one zero at $x = +W/2$ corresponding to the argument $(k \pm l \pm N)\pi$. This explains that every other element is zero when integration between $\mp N\pi$ and $(k \pm l \pm N)\pi$ takes place on an even number of integrand antinodes ($k \pm l \pm 2N$ even implies $k \pm l$ even).

Apart from this true selection rule, we have a "mild" rule to identify the strongest terms, i.e., those corresponding to the modes experiencing the strongest interaction. The integrals of individual terms give the largest nonzero absolute value when they correspond to a single antinode on the integration domain, hence the generic "strongest coupling selection rule,"

$$k \pm l \pm 2N = \pm 1. \tag{7}$$

Equation (7) gives the basis to explain the structure of Fig. 3(a) and the full system of Fig. 2. For instance, the two dark red arrows highlight an oblique line of matrix elements with much higher values than their neighbors, indicating that the k and l modes involved in each of these elements interact preferentially. It is easy to verify that these modes follow the rule given by Eq. (7) if one remembers that the $\mathcal{PT}$-symmetry profile chosen here is $2N = 6$: Their indices verify $k + l = 7$, or equivalently, $k + l = 2N + 1$. We can thus state that preferential interactions occur among modes 3 and 4, modes 2 and 5, and modes 1 and 6, just as in the full system of Fig. 2 where an EP between modes 3 and 4 is followed by EPs between modes 2 and 5 and modes 1 and 6, respectively.

There is some more complexity due to the presence of four terms from Eq. (6), connected to the order of the three interactions, but the essence of the structure of Fig. 3(a) lies in this selection rule. Higher harmonic components of $f(x)$, such as $f_p(x) \equiv \sin(2\pi pNx/W)$ within a prefactor intervene simply by the substitution $k \pm l \pm (2pN) = \pm 1$ in Eq. (7), creating more patterns with the $2N$ periodicity.

It is easy to numerically compute the perturbative eigenvalues using Eq. (4) as performed in Fig. 3(b). The sixfold pattern of the full system of Fig. 2 is well reproduced for the first six modes, and the ordering of crossing of modes of opposite curvatures is in the observed order [(3,4),(2,5),(1,6)]. Further modes are also grouped in a similar way, but the figures are rather complex and do not render this very clearly.

To conclude this section, a second-order perturbative analysis performed on a generic FN coupling array explains the formation of clusters of six modes for the full system of Fig. 2. We will now extract more useful information from the same waveguide array problem with an exact resolution that will include exceptional points at mode crossings.

IV. EXCEPTIONAL POINTS IN THE WAVEGUIDE ARRAY MODEL

We can easily extract the evolution of real and imaginary parts of the eigenvalues as a function of $\Delta\omega_I$ as well as the locus (trajectory) followed by them in the complex plane. A typical case is shown in Fig. 4.

We see that the coincidence with the true multimode waveguide calculation of Fig. 2 is achieved to a high degree. Of course, the clusters are exactly the same; they stem from the system's symmetry. The real part trajectories, for instance how they merge at the succession of EPs of the first and second clusters, are quite well reproduced, including the inflections. The evolution of the imaginary parts presents similar trends. At this stage, it is interesting to tune the model in order to test either the degree of resemblance that can be attained or the influence of physical parameters.
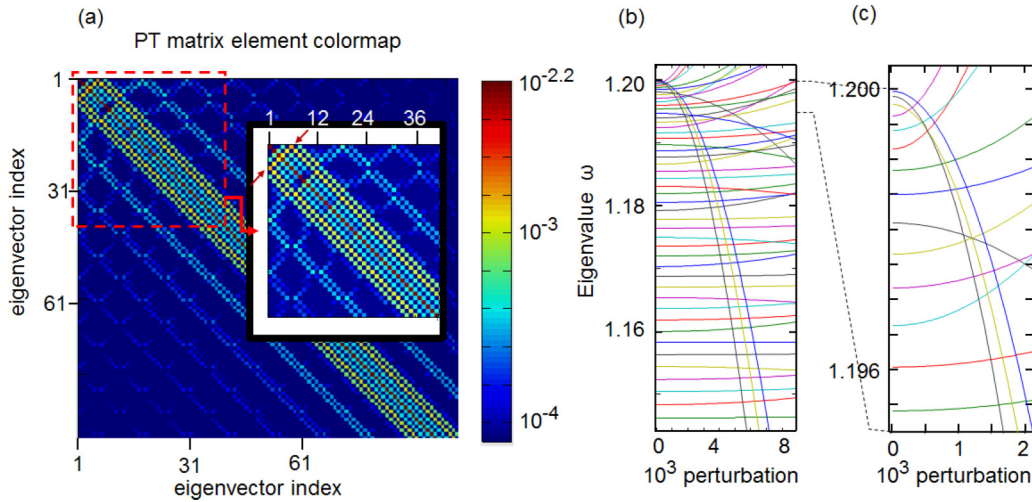
FIG. 3. (Color online) (a) Color plot of the $\sim100 \times 100$ squared matrix elements D_{kl} of the $\mathcal{PT}$ perturbation $V \equiv V_{\mathcal{PT}}$ for $N = 6, M = 204$, the scaling of $V_{\mathcal{PT}}$ to κ making the quantity dimensionless; the color map is based on $\log_{10}(|D_{kl}|)$. The inset shows the 40 first modes with every other element vanishing (selection rule $k + l$ odd) and the two dark red arrows at the top left corner point the line $k + l = 7 = N + 1$ with the strongest interaction, (b) perturbation induced eigenvalues for the $\sim$50 top eigenvalues by a growing $\mathcal{PT}$-symmetric potential (abscissa $= \mathcal{PT}$ perturbation strength), and (c) detail for the 14 top ones, showing the trend of perturbed modes to group into clusters of $N = 6$ elements.

For this, we test a simple modification of the gain or loss profile by imposing, instead of a constant f_j, a gain or loss profile with a strength increasing or decreasing from the guide center to its edges with a parabolic trend: $f_j = $ $\pm[1 + \alpha(j/M - 1/2)^2]$ with $\alpha = 1$ for instance or $\alpha = -1$. This operation would be lengthy to reproduce for the true multimode waveguide by the transmission matrix method (TMM) as would a cosine modulation discussed next.
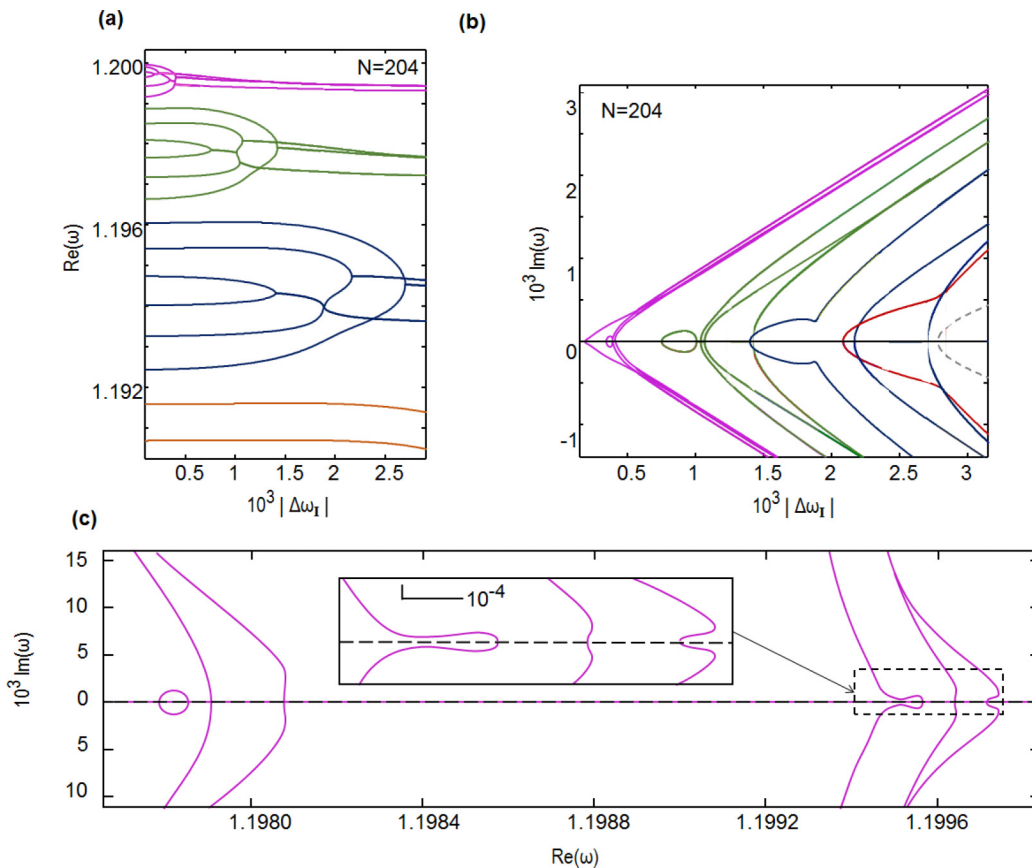

FIG. 4. (Color online) Eigenvalue vs gain or loss parameters using here $N = 204$ (a) Re(ω) vs $\Delta\omega_I$, (b) Im(ω) vs $\Delta\omega_I$, and (c) trajectory of in complex plane for the ten first eigenvalues with a zoom on the first cluster.
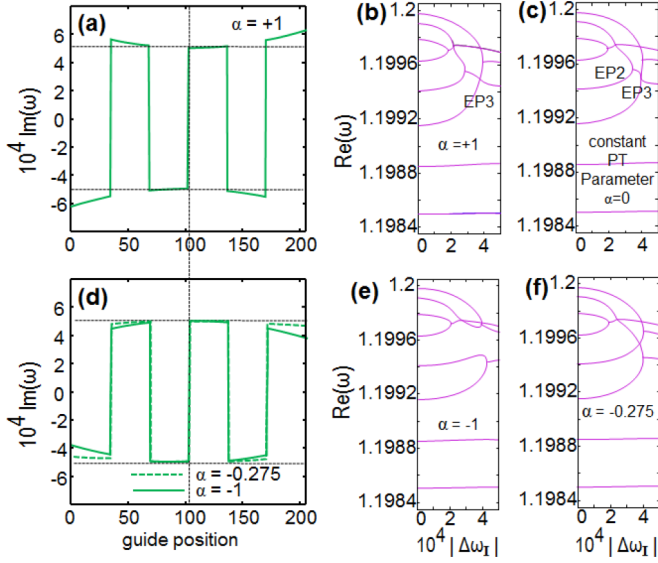
FIG. 5. (Color online) (a) Profile of the gain or loss distribution across the guide, based on $|\Delta\omega_I| = 5 \times 10^{-4}$ for a case with more gain on the edges ($\alpha = 1$), (b) Re(ω) vs $\Delta\omega_I$ for the configuration $\alpha = 1$ in (a), (c) comparison to the constant gain or loss profile case ($\alpha = 0$); note that the first EP is more separated and the next one more clustered than in (b), (d) the same in the case of depleted gain or loss on the edges: $\alpha = -1$ (solid line) and $\alpha = -0.275$ (dashed line), (e) for $\alpha = -1$, the set of higher EPs now has a different topology with adjacent mode pairing, and (f) the limit case is found at $\alpha = -0.275$ and has an eigenvalue crossing pattern.
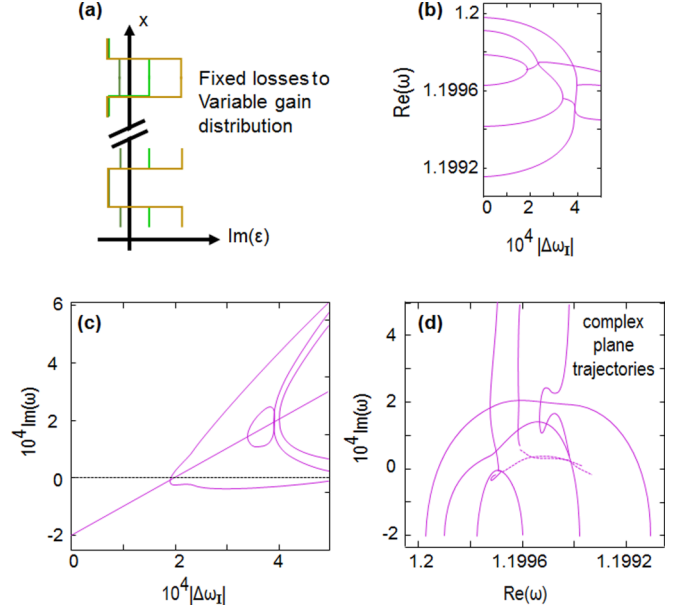

FIG. 6. (Color online) Case of constant losses and variable gain as illustrated by the profile in (a). (b) Real part and (c) imaginary part of the eigenvalues with on this latter the overall positive slope. The most affected plot is that of the complex plane (d), stemming mainly from the overall growth of gain in the imaginary part (c), whereas the real part (b) is essentially similar to the balanced gain or loss case.

In Fig. 5 we illustrate the effect of the parameter α on the first cluster(s), focusing on the real part and the shape around the successive EPs. We can see how the clustering evolves through the role of the intermediate EP located at point EP2. As we tune the curvature parameter α down from $\alpha = 1$ to $\alpha = 0$, EP2 approaches the upper curves that give rise to EP3. If we go to negative α, EP2 splits this curve, around $\alpha = -0.275$, Fig. 5(f) so that the two EPs now arise along the curves of two adjacent modes. Beyond this point, at $\alpha = -1$, Fig. 5(e), the clustering does not have the same topology. Hence, there is some tolerance on the exact profile of gain or loss, but going too far can change the topology of the EP and affect the operation in terms of device physics rather profoundly.

We next examine the possibility of introducing a constant loss (or gain) factor for one of the subsets, while keeping the other tunable with variable gain (see Fig. 6). This is a situation we have pointed out to implement $\mathcal{PT}$ symmetry with plasmonics [8–10]. Indeed, for an adequate value of the constant loss factor, here $-|\Delta\omega_I| = -2 \times 10^{-4}$, the first EP can be pulled nearly onto the real axis [Im(ω_{EP}) $\sim$ 0]. The local evolution of the eigenvalues remains mostly similar to the previous case so that the singularities can in principle be exploited on a similar basis. A gauge transform is known to connect in general unbalanced versions to balanced versions of $\mathcal{PT}$ symmetry [10], and it is likely that an ansatz of this gauge transform also works here. Note however that the diagram in the complex plane becomes more intricate.

V. MODE PAIR SELECTION IN THE $\mathcal{PT}$-SYMMETRIC BROAD WAVEGUIDE WITH TRANSVERSE PERIODICITY

We now turn to the possible application of $\mathcal{PT}$ symmetry to modal selection in broad waveguides, using still the simplified array model. The input modes are supposed to be the familiar eigenmodes of the lossless(or gainless) system with a (scalar) profile essentially given by $E_m(x) = E_o \sin(\pi m x / W)$, which holds well for all low-order modes that do not leak much outside the guide.

We project one such mode $|m\rangle$ onto the eigenmodes $|p\rangle$ of the system in the presence of the gain and loss pattern. We then evolve each mode with its complex exponential behavior $\exp(i\omega_p z)$, reminding that we noted the eigenvalues ω in order to get analogies but that they are indeed propagation constants along the guide z. We just look at the result in terms of intensity after a finite length with the aim of direct detection in mind: The system is highly nonconservative and does not seem yet to lend itself well to the ideal drop function whereby all nonselected modes would be unaffected. We typically use a length L such that the gain-length product gL brings a reference gain of 20 or 40 dB, a value certainly overestimated in terms of effective gain since $\mathcal{PT}$ symmetry demands propagation in both gain and loss media; but it is eventually high enough to distinguish signals and give a first look at the issue of cross-talk behavior.

The central idea is to operate just above an EP so that there is a large gain difference with the other nearby modes due to the abrupt behavior of the eigenvalues in the EP's vicinity. We apply here this idea using a case where 8 layers + 2 half-layers alternating gain and loss are present across the waveguide, corresponding to $N = 4.5$ periods and a variation $f(x) \equiv$
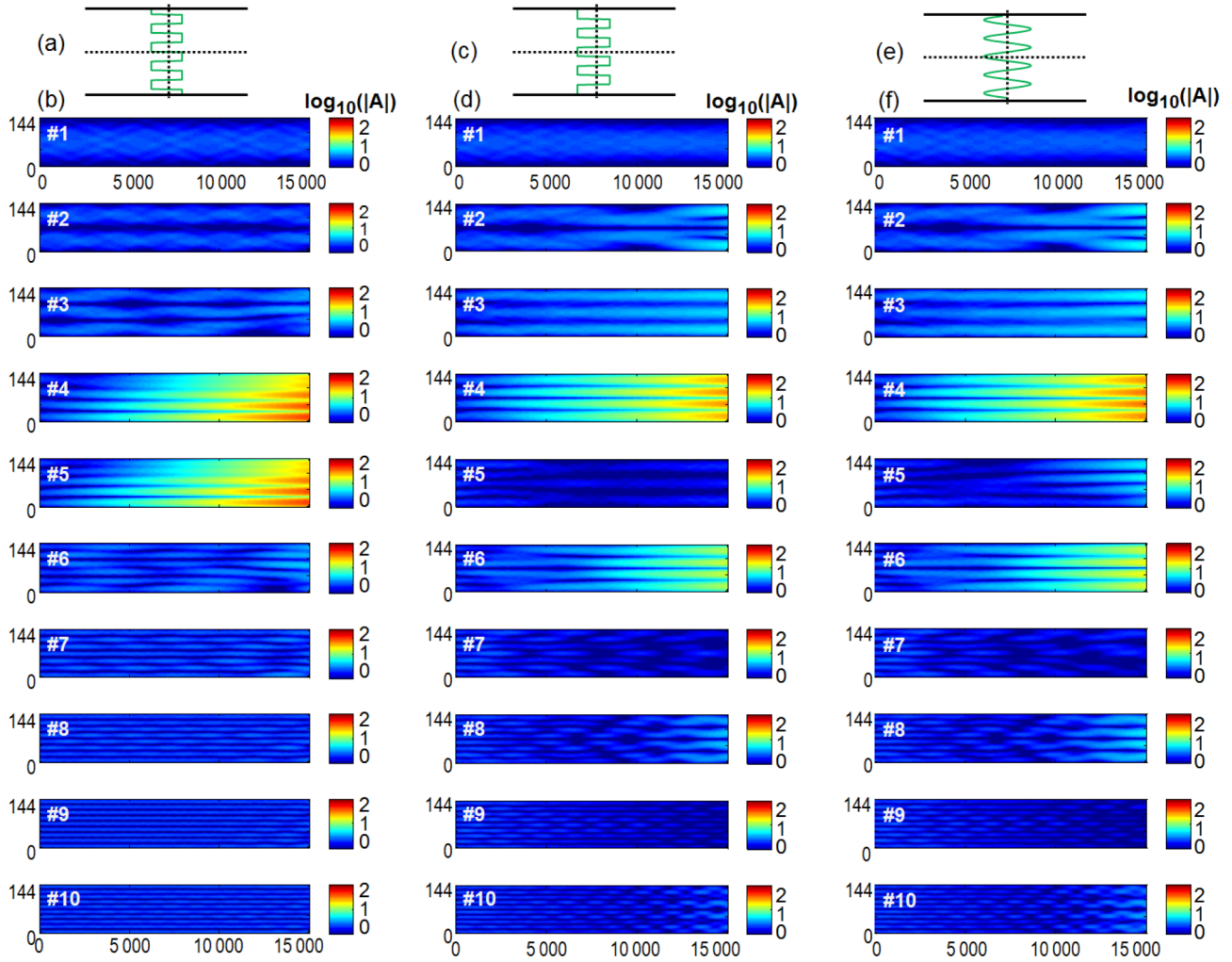
FIG. 7. (Color online) Spatial evolution of basic waveguide modes 1–10 submitted to various gain or loss patterns: (a) the $\mathcal{PT}$-symmetric $\Delta\omega_I$ profile with unit widths $W/9$, selecting in (b) modes 4 and 5 and leaving others at nearly zero gain, (c) the same square function but in a symmetric version, thus suited for mode 4 in the series of nine modes tested in (d). Note the modest rejection of modes 2, 6, and 7, and (e) and (f) the same as (c) and (d) with a sinusoidal $\Delta\omega_I$ profile. The rejection is poorer than in (c) and (d).

$\mathrm{sgn}[\sin(9\pi x/W)]$ within a scalar factor. Because we consider an odd number of layers in this example, each section with gain or loss in the transverse direction has a dimension $W/9$ except for the external layers which have a size of only $W/18$. For our simplified waveguide array model, we now need to use a total number of modes of a multiple of 9 and even, here $M = 144$ to get perfect compatibility with this periodicity and the $\mathcal{PT}$ symmetry.

With our dimensionless amplitude gain values $\Delta\omega_I$ of 5.5 $\times 10^{-3}$ per unit length, we use a length of 1.5×10^4 formal units, thus $\Delta\omega_I L$ is around 50, corresponding to nearly 20 dB of intensity for the amplified cases a little above the first EP as we will see.

Figure 7 shows the fate of the ten first modes injected separately in the broad waveguide and submitted to three different $\Delta\omega_I(x)$ profiles. In Fig. 7(b) is the case of the $\mathcal{PT}$-symmetric profile shown in Fig. 7(a). Only two modes are clearly selected, modes 4 and 5, and it can be seen that they evolve toward the same transverse profile on the right end of the waveguide with more power at the bottom (small x). To

understand this behavior, we plot in Figs. 8(a)–8(c) the same information on the eigenvalue spectrum and complex plane location as in the above Fig. 4 for instance. Notice that the modulation with $2N = 9$ elements now results in a clustering of eight modes per cluster. We have set an upper limit between the first and the second EP: We see from Figs. 8(a) and 8(b) that modes 4 and 5 have just gone above their EP and have thus become complex-conjugated values. One of them is a gain mode, and the other is a loss mode. Their amplitude and phase profile are given in Figs. 8(d) and 8(e) with expected symmetries. We see that the gain mode has its lobes on the low x side of the waveguide where there is more gain than on the opposite large x side. The favored mode of Fig. 7(b) is just the gain mode. Upon projecting modes 4 and 5 of the non-$\mathcal{PT}$ system, it is clear from the profiles that both eigenmodes of Fig. 8 are generated but only the gain one strengthens upon propagation, whereas the other one decays. An in-depth analysis of the fringe pattern at the start of the propagation would make this fully explicit and could offer some interest in other contexts.
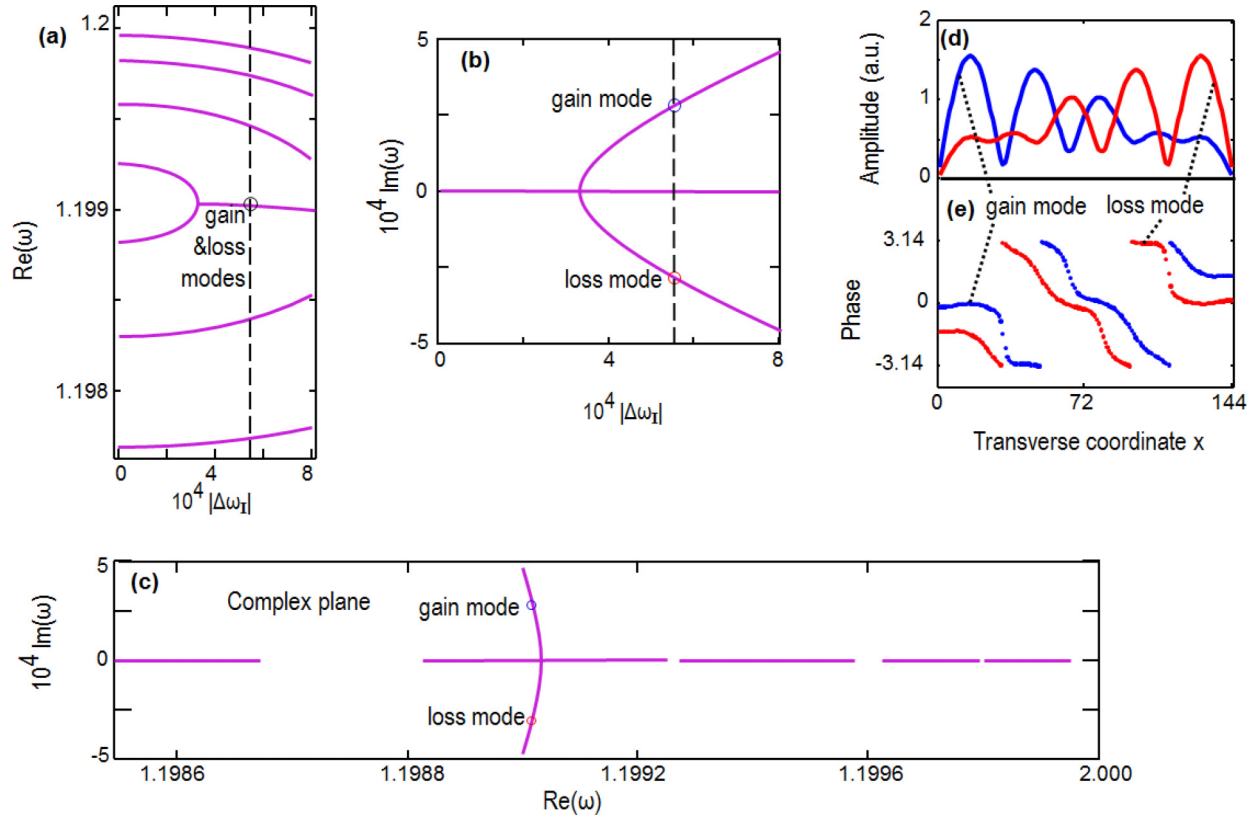
FIG. 8. (Color online) Eigenvalues as a function of $\Delta\omega_I$: (a) real part with the first EP apparent at $\Delta\omega_I \sim 3.3 \times 10^{-4}$, (b) imaginary part with the same EP, (c) eigenvalue trajectories and EP in the complex plane, (d) amplitude profiles along x of the gain and loss modes evidenced in Fig. 7 and pointed by the circles in (a)–(c), (e) phase profiles of the same modes.

In other words, the fact that two modes are amplified, while not a strict single-mode selection mechanism, is a direct consequence of the above-EP system eigenstates with only the gain mode emerging after enough propagation. The other modes of Fig. 7(a) are very silent, remaining essentially at their entrance level: They all feel the compensating influence of gain and loss across the two signs taken by $\Delta\omega_I(x)$ because they are far below their own EP and thus remain essentially identical to the injected modes [see Figs. 8(a) and 8(b)]. By the same token, there is very little interaction between the silent modes (or between the silent modes and modes 4 and 5) because they essentially remain a set of orthogonal solutions just as the injected modes. It is not our purpose here to quantify the selectivity as the metrics need to be worked out in a given context to be really significant. But this apparent selectivity is a good omen for the general use of $\mathcal{PT}$ symmetry in this modal selection spirit.

Comparatively, if we implement similar gain or loss values but with a profile $\Delta\omega_I(x)$ that is plainly symmetric with the same transverse periodicity, i.e., $W/9$ elements, we see in Fig. 7(b) that now only one mode emerges from the competition, mode 4. This result is expected as this is the only mode whose four antinodes can approximately coincide with the four gain stripes in $\Delta\omega_I(x)$. But we also see that it is hard to achieve selectivity. The modest rejection of modes 2, 6, and 7 seems difficult to avoid, $\Delta\omega_I(x)$ having Fourier components that favor these other modes. Since an

electromagnetic problem, such as this one, is not linear with respect to dielectric modulation (all the more if we additionally operate above the EP), there is no obvious orthogonality that can grant selective amplification of a given mode from such a case. As a simple attempt at minimizing the Fourier spectrum of the modulation $\Delta\omega_I(x)$, we show in Fig. 7(e) the case of a sinusoidal modulation of $\Delta\omega_I(x)$. The effect is to make rejection even worse, see Fig. 7(f).

It is of course delicate to extrapolate from this particular example. An optimal strategy for $\Delta\omega_I(x)$ with selectivity as a figure of merit could well be none of the proposed solutions. On the other hand, homing in on good solutions from the start is certainly welcome to understand what opportunities are provided by these $\mathcal{PT}$-symmetric systems. Here, we are operating with overall gains on the order of 15 dB, and the rejection of nonselected modes (among the ten first modes) is about 13–15 dB for the $\mathcal{PT}$-symmetric case, whereas it drops to half this value for the symmetric profile $\Delta\omega_I(x)$.

VI. CONCLUSION

In conclusion, we have studied a broad waveguide with the issue of selecting one of its modes by a transverse modulation of gain and loss in mind. We have analyzed the mode clustering of a real system and shown that it was equivalent to that of a more easily resolved first-neighbor model. We have provided a perturbation analysis to second order and worked out the

relevant quasiselection rules to explain that clustering. From the point of view of the fate of field distributions entering such a broad waveguide, we have succeeded to isolate a pair of modes with a high rejection in the case of a $\mathcal{PT}$-symmetric profile. Conversely, we have not been able, by a substantial amount, to get a similar rejection with a symmetric profile. We cannot ascribe yet an exact analytical theory to account for rejections above the EP among other aspects, but we have enough confidence in the validity of the scheme we propose to conjecture that it could be exploited with good generality in any generic multimode guiding systems that can support gain with transverse spatial modulation.

We also note that optical signal processing between an input and an output plane may be envisioned from any mix of modal and nonmodal points of view. For instance, the scope of devices, such as MMIs (based on broad waveguides) is a spatial imaging operation, not a modal one. A very general task, analogous to defining a signal processing operation in the general time-frequency domain (wavelet based for instance), could be a mix of spatial and modal requirements. We did not wish to be excessively general for the time being and only explored here a $\mathcal{PT}$-symmetric broad waveguide system with a view to its modal behavior, and we have found very encouraging features in this respect.

[1] C. M. Bender and S. Boettcher, Real spectra in non-Hermitian Hamiltonians having PT-symmetry, Phys. Rev. Lett. **80**, 5243 (1998).

[2] C. M. Bender, Making sense of non-Hermitian Hamiltonians, Rep. Prog. Phys. **70**, 947 (2007).

[3] H. P. Nolting, G. Sztefka, M. Grawert, and J. Ctyroky, Wave propagation in a waveguide with a balance of gain and loss, in *Integrated Photonics Research*, Vol. 6 of 1996 OSA Technical Digest Series (Optical Society of America, 1996), paper IMD5.

[4] S. Klaiman, U. Günther, and N. Moiseyev, Visualization of branch points in PT-symmetric waveguides, Phys. Rev. Lett. **101**, 080402 (2008).

[5] A. Guo, G. J. Salamo, D. Duchesne, R. Morandotti, M. Volatier-Ravat, V. Aimez, G. A. Siviloglou, and D. N. Christodoulides, Observation of PT-symmetry breaking in complex optical potentials, Phys. Rev. Lett. **103**, 093902 (2009).

[6] B. Peng, Ş. K. Özdemir, F. Lei, F. Monifi, M. Gianfreda, G. L. Long, S. Fan, F. Nori, C. M. Bender, and L. Yang, Parity–time-symmetric whispering-gallery microcavities, Nat. Phys. **10**, 394 (2014).

[7] Y. Yan and N. C. Giebink, Passive PT Symmetry in Organic Composite Films via Complex Refractive Index Modulation, Adv. Opt. Mater. **2**, 423 (2014).

[8] H. Benisty, A. Degiron, A. Lupu, A. De Lustrac, S. Chenais, S. Forget, M. Besbes, G. Barbillon, A. Bruyant, S. Blaize, and G. Lerondel, Implementation of PT symmetric devices using plasmonics: Principle and applications, Opt. Express **19**, 18004 (2011).

[9] H. Benisty, C. Yan, A. Degiron, and A. Lupu, Healing near-PT-symmetric structures to restore their characteristic singularities: analysis and examples, J. Lightwave Technol. **30**, 2675 (2012).

[10] A. Lupu, H. Benisty, and A. Degiron, Switching using PT-symmetry in plasmonic systems: positive role of the losses, Opt. Express **21**, 21651 (2013).

[11] M. Kulishov, J. M. Laniel, N. Bélanger, J. Azaña, and D. V. Plant, Nonreciprocal waveguide Bragg gratings, Opt. Express **13**, 3068 (2005).

[12] M. Kulishov, J. M. Laniel, N. Bélanger, and D. V. Plant, Trapping light in a ring resonator using a grating-assisted coupler with asymmetric transmission, Opt. Express **13**, 3567 (2005).

[13] Z. Lin, H. Ramezani, T. Eichelkraut, T. Kottos, H. Cao, and D. N. Christodoulides, Unidirectional invisibility induced by PT-symmetric periodic structures, Phys. Rev. Lett. **106**, 213901 (2011).

[14] A. Lupu, H. Benisty, and A. Degiron, Using optical PT-symmetry for switching applications, Photonics Nanostruct. Fundam. Appl. **12**, 305 (2014).

[15] L. Feng, M. Ayache, J. Huang, Y.-L. XU, M.-H. Lu, Y.-F. Chen, Y. Fainman, and A. Scherer, Nonreciprocal light propagation in a silicon photonic circuit, Science **333**, 729 (2011).

[16] C. E. Rüter, K. G. Makris, R. El-Ganainy, D. N. Christodoulides, M. Segev, and D. Kip, Observation of parity-time symmetry in optics, Nat. Phys. **6**, 192 (2010).

[17] K. G. Makris, R. El-Ganainy, D. N. Christodoulides, and Z. H. Musslimani, Beam Dynamics in PT Symmetric Optical Lattices, Phys. Rev. Lett. **100**, 103904 (2008).

[18] J. Ctyroky, V. Kuzmiak, and S. Eyderman, Waveguide structures with antisymmetric gain/loss profile, Opt. Express **18**, 21585 (2010).

[19] V. V. Konotop, V. S. Shchesnovich, and D. A. Zezyulin, Giant amplification of modes in parity–time symmetric waveguides, Phys. Lett. A **376**, 2750 (2012).

[20] A. Regensburger, C. Bersch, M.-A. Miri, G. Onishchukov, D. N. Christodoulides, and U. Peschel, Parity–time synthetic photonic lattices, Nature (London) **488**, 167 (2012).

[21] A. A. Sukhorukov, S. V. Dmitriev, S. V. Suchkov, and Y. S. Kivshar, Nonlocality in PT-symmetric waveguide arrays with gain and loss, Opt. Lett. **37**, 2148 (2012).

[22] D. A. Zezyulin and V. V. Konotop, Nonlinear modes in finite-dimensional PT-symmetric systems, Phys. Rev. Lett. **108**, 213906 (2012).

[23] S. Longhi, PT-symmetric laser absorber, Phys. Rev. A **82**, 031801(R) (2010).

[24] Y. D. Chong, L. Ge, and A. D. Stone, PT-symmetry breaking and laser-absorber modes in optical scattering systems, Phys. Rev. Lett. **106**, 093902 (2011).

[25] H. Hodaei, M.-A. Miri, M. Heinrich, D. N. Christodoulides, and M. Khajavikhan, Parity-time–symmetric microring lasers, Science **346**, 975 (2014).

[26] Y. N. Joglekar, C. Thompson, D. D. Scott, and G. Vemuri, Optical waveguide arrays: quantum effects and PT symmetry breaking, Eur. Phys. J.: Appl. Phys. **63**, 30001 (2013).

[27] M. C. Zheng, D. N. Christodoulides, R. Fleischmann, and T. Kottos, PT optical lattices and universality in beam dynamics, Phys. Rev. A **82**, 010103 (2010).

[28] L. Feng, X. Zhu, S. Yang, H. Zhu, P. Zhang, X. Yin, Y. Wang, and X. Zhang, Demonstration of a large-scale optical exceptional point structure, Opt. Express **22**, 1760 (2014).

[29] G. P. Tsironis and N. Lazarides, PT-symmetric nonlinear metamaterials and zero-dimensional systems, Appl. Phys. A: Mater. Sci. Process. **115**, 449 (2014).

[30] I. V. Barashenkov, L. Baker, and N. V. Alexeeva, PT-symmetry breaking in a necklace of coupled optical waveguides, Phys. Rev. A **87**, 033819 (2013).

[31] O. Bendix, R. Fleischmann, T. Kottos, and B. Shapiro, Exponentially Fragile PT Symmetry in Lattices with Localized Eigenmodes, Phys. Rev. Lett. **103**, 030402 (2009).

[32] D. D. Scott and Y. N. Joglekar, Degrees and signatures of broken PT-symmetry in nonuniform lattices, Phys. Rev. A **83**, 050102 (2011).

[33] D. E. Pelinovsky, D. A. Zezyulin, and V. V. Konotop, Nonlinear modes in a generalized PT-symmetric discrete nonlinear Schrödinger equation, J. Phys. A: Math. Theor. **47**, 085204 (2014).

[34] P. Kevrekidis, D. Pelinovsky, and D. Tyugin, Nonlinear Stationary States in PT-Symmetric Lattices, SIAM J. Appl. Dyn. Syst. **12**, 1210 (2013).

[35] R. Halir, I. Molina-Fernandez, A. Ortega-Monux, J. G. Wanguemert-Perez, D.-X. Xu, P. Cheben, and S. Janz, A Design Procedure for High-Performance, Rib-Waveguide-Based Multimode Interference Couplers in Silicon-on-Insulator, J. Lightwave Technol. **26**, 2928 (2008).

[36] A. Maese-Novo, R. Halir, S. Romero-Garcia, D. Perez-Galacho, L. Zavargo-Peche, A. Ortega-Monux, I. Molina-Fernandez, J. G. Wanguemert-Perez, and P. Cheben, Wavelength independent multimode interference coupler, Opt. Express **21**, 7033 (2013).

[37] V. Liu, D. A. B. Miller, and S. Fan, Ultra-compact photonic crystal waveguide spatial mode converter and its connection to the optical diode effect, Opt. Express **20**, 28388 (2012).

[38] S.-Y. Tseng and X. Chen, Engineering of fast mode conversion in multimode waveguides, Opt. Lett. **37**, 5118 (2012).

[39] L.-W. Luo, N. Ophir, C. P. Chen, L. H. Gabrielli, C. B. Poitras, K. Bergmen, and M. Lipson, WDM-compatible mode-division multiplexing on a silicon chip, Nat. Commun. **5**, 3069 (2014).

[40] U. Peschel, T. Pertsch, and F. Lederer, Optical Bloch oscillations in waveguide arrays, Opt. Lett. **23**, 1701 (1998).

[41] D. N. Christodoulides, F. Lederer, and A. Silberberg, Discretizing light behaviour in linear and nonlinear waveguide lattices, Nature (London) **424**, 817 (2003).

[42] N. Belabas Plougonven, C. Minot, G. Bouwmans, A. Levenson, and J.-M. Moison, Discrete photonics resonator in coupled waveguide arrays, Opt. Express **22**, 12379 (2014).

[43] C. Pierre, Weak and strong vibration localization in disordered structures: a statistical investigation, J. Sound Vib. **139**, 111 (1990).

[44] H. Benisty, Reduced electron-phonon relaxation rates in quantum-box systems: theoretical analysis, Phys. Rev. B **51**, 13281 (1995).